

## Time series data correction for the Chang'E-1 gamma-ray spectrometer \*

Li-Yan Zhang<sup>1,2</sup>, Yong-Liao Zou<sup>1</sup>, Jian-Zhong Liu<sup>1</sup>, Jian-Jun Liu<sup>1</sup>, Ji Shen<sup>1</sup>, Ling-Li Mu<sup>1</sup>, Xin Ren<sup>1</sup>, Wei-Bin Wen<sup>1</sup> and Chun-Lai Li<sup>1</sup>

<sup>1</sup> National Astronomical Observatories, Chinese Academy of Sciences, Beijing 100012, China; [zhangly@nao.cas.cn](mailto:zhangly@nao.cas.cn)

<sup>2</sup> Graduate University of Chinese Academy of Sciences, Beijing 100049, China

Received 2010 July 15; accepted 2011 January 6

**Abstract** The main goal of the gamma-ray spectrometer (GRS) onboard Chang'E-1 (CE-1) is to acquire global maps of elemental abundances and their distributions on the moon, since such maps will significantly improve our understanding of lunar formation and evolution. To derive the elemental maps and enable research on lunar formation and evolution, raw data that are received directly from the spacecraft must be converted into time series corrected gamma-ray spectra. The data correction procedures for the CE-1 GRS time series data are thoroughly described. The processing procedures to create the time series gamma-ray spectra described here include channel processing, optimal data selection, energy calibration, gain correction, dead time correction, geometric correction, orbit altitude normalization, eliminating unusable data and galactic cosmic ray correction. Finally, descriptions are also given on data measurement uncertainties, which will help the interested scientists to understand and estimate various uncertainties associated with the above data processing.

**Key words:** instrumentation: spectrographs (gamma-ray spectrometer) — gamma-rays: observations — methods: data analysis

### 1 INTRODUCTION

The gamma-ray spectrometer (GRS) is one of the main payloads onboard Chang'E-1 (CE-1). Its main scientific objectives are to analyze the abundances and distributions of useful elements on the lunar surface, to study the distribution of lunar resources like rocks, minerals, etc., and to find enriched areas of utilizable resources together with the imaging interferometer and X-ray spectrometer onboard CE-1, in order to improve our understanding of lunar formation and evolution. To achieve the above-mentioned scientific objectives, it is important that raw data that are received directly from CE-1 GRS be converted into fully corrected time-ordered gamma-ray spectra that are used to directly derive elemental maps. In this paper, we provide a thorough description of the data correction processes for the CE-1 GRS time series data, which will provide a foundation for future Chinese lunar gamma-ray experiments that need to carry out similar processing steps and help interested scientists to understand and estimate the data correction procedures and methods, and various uncertainties associated with the processing for better using the corrected data to carry out research on lunar surface composition, lunar origin and evolution.

---

\* Supported by the National Natural Science Foundation of China.

The data correction processing methods described in the paper to create the CE-1 GRS time series gamma-ray spectra include channel processing, the optimal data selection from two data acquisition stations, energy calibration, gain correction, dead time correction, geometric correction, orbit altitude normalization, eliminating unusable data and galactic cosmic ray correction. Before time series data correction is described, a brief review of the CE-1 GRS sensor operation and data collection modes is provided. We also review and summarize the additional auxiliary data sets that are used for the CE-1 GRS data correction. In the last section of the paper, descriptions are given of data measurement uncertainties inherent in the time series data before and after the data processing.

## 2 CE-1 GRS SENSOR AND SUPPORT INFORMATION

### 2.1 Review of the CE-1 GRS Sensor

CE-1 GRS was designed and developed by the Purple Mountain Observatory, Chinese Academy of Science (CAS). It consists of a gamma-ray detector (GRD) and electronics control box (ECB) (Chang et al. 2009) as shown in Figure 1 (a) and (b). As shown in Figure 1 (b), GRD includes a central prime crystal, surrounding anticoincidence crystal, one 5'' photomultiplier tube (PMT) and two 3'' PMTs (Chang et al. 2009). The prime crystal is an 11.8 cm diameter by a 7.8 cm long cylinder of CsI (Tl) crystal. It measures gamma-rays with energies from 0.3 to 11.2 MeV. The measured energy resolution is 8.27% at 0.662 MeV and operates in  $E^{-1/2}$  (where  $E$  = gamma-ray energy). The side and back of the prime crystal is surrounded by a well type CsI (Tl) crystal shield with thickness of about 3 cm. The 5'' PMT collects gamma-rays from the prime crystal, and the two 3'' PMTs collect gamma-rays from the anticoincidence crystal. In lunar orbit, the efficiency of the anticoincidence system's background rejection is almost 70%.

CE-1 operates in a circular lunar polar orbit with inclination of approximately 90 degrees with respect to the lunar equatorial plane at a height of about 200 km above the lunar surface, and it adopts a three-axis stabilized attitude control. GRS is installed in the corner of the spacecraft, and cannot be shielded by any large-sized or high-quality component of the spacecraft within the range of  $-60^\circ \sim +60^\circ$  in its field of view. GRS is an uncollimated, omnidirectional gamma-ray detector. It includes one prime detector and one anticoincidence detector. The prime detector collects a spectrum with 512 channels every three seconds originating from the moon and other non-lunar sources. The anticoincidence detector collects a spectrum with 256 channels every second originating from the absorption of Compton-scattered gamma-rays from the spacecraft, and whose primary objective is to reduce the spacecraft's background gamma-rays striking the prime detector. The data collection circuit of GRS uses the anticoincidence procedure to eliminate the anticoincidence signals and measure the lunar gamma-ray spectra. The collected data are then transmitted to the ground from CE-1 and are used to obtain the elemental abundances on the lunar surface through data analysis.

GRS started its first observation of the lunar gamma-ray spectra at 19:58 on 2007 Nov. 27 (UTC). During the duration of the CE-1 mission, the working times of GRS are shown in Table 1.

**Table 1** Working Times of CE-1 GRS

No.	Beginning time (UTC)	End time (UTC)
1	2007-11-27 T19:58	2007-12-01 T02:22
2	2007-12-04 T01:27	2008-01-26 T22:56
3	2008-01-30 T00:59	2008-02-06 T00:38
4	2008-05-15 T11:28	2008-07-03 T02:30
5	2008-07-03 T02:30	2008-07-25 T11:20
6	2008-11-21 T06:16	2008-11-21 T23:29

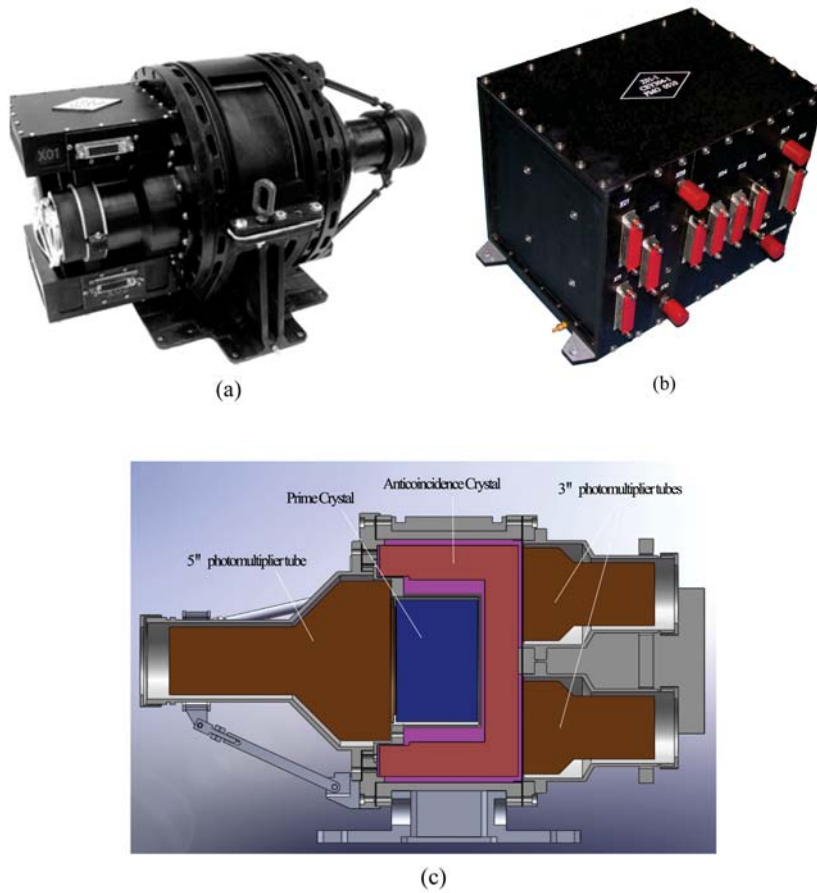


**Fig. 1** (a) GRD, (b) the electric control box and (c) the structure of GRD.

## 2.2 Auxiliary Data

In addition to the two fundamental spectra from the prime detector and the anticoincidence detector, a number of other auxiliary CE-1 data products and data sets are used in the GRS analysis. They include the engineering and telemetry parameters of GRS, spacecraft ephemeris and attitude data, GRS installation parameters on the spacecraft and ground calibration data of GRS.

The engineering and telemetry parameters for the GRS analysis include the sensor temperature and the high voltage. The sensor temperature is a measurement of GRS housing temperature and is measured once per second. The high voltage (HV) measurements monitor the combined HV on each of the three PMTs once per second, that include one PMT of the prime detector and two PMTs of the anticoincidence detector. During the mission, the HV could be changed to keep the gain for each PMT within an acceptable range.

The spacecraft's ephemeris data include spacecraft positions and speeds of  $X$ ,  $Y$  and  $Z$  axes in the J2000 geocentric coordinate system. The spacecraft's attitude data include three Euler attitude angles that are yaw, roll and pitch angle. The spacecraft ephemeris and attitude data are used to calculate lunar positions of measured spectra and GRS sensor observation angles.

The GRS installation parameters include the instrument coordinates and angles of the  $X$ ,  $Y$  and  $Z$  axes in the spacecraft body's coordinate system.

The ground calibration data include the laboratory calibrations and numerical simulations of GRS. The ground calibrations are used to acquire 1) detector energy linearity, resolution and range, 2) effective area and detection efficiency of the GRS detector as a function of energy, 3) gain calibration, 4) angle calibration, 5) temperature influence on the energy linearity and resolution, 6) dead time calibration, 7) anticoincidence counting rate influence on the dead time of the prime detector, and 8) efficiency of anticoincidence background rejection.

### 3 PRIMARY PROCESSING

In this section, we describe the primary processing that is carried out on the CE-1 GRS data. This processing includes steps (Fig. 2) such as channel processing, optimal data selection, system correction, geometric corrections, orbit altitude normalization, unusable data elimination and galactic cosmic ray correction. The final result is a fully corrected time series data set that is ready for spectral analysis, mapping, and abundance calculations (Metzger et al. 1974, 1977, 1979; Metzger 1993; Lawrence et al. 1998, 2004; Prettyman et al. 2006).

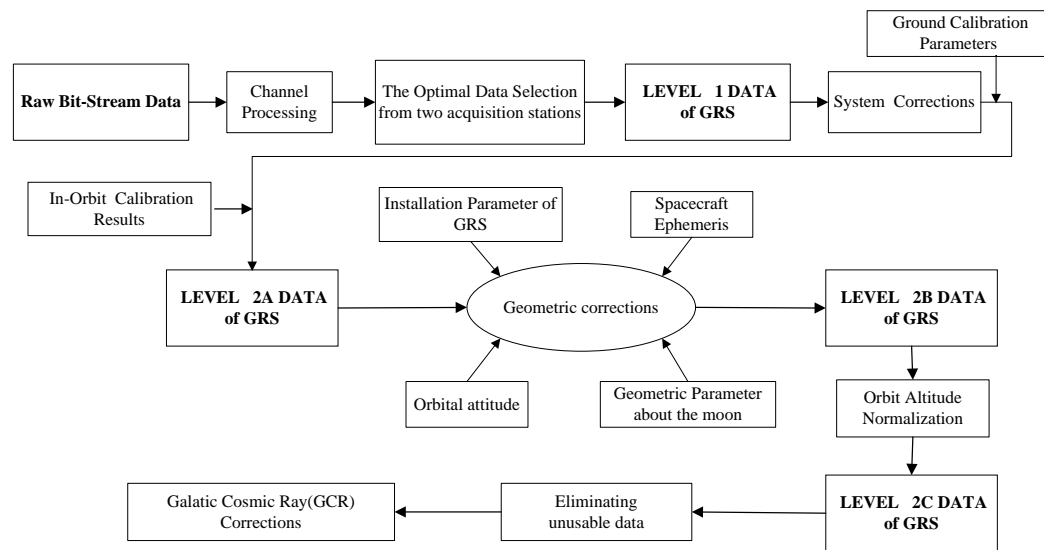


Fig. 2 Procedure of time series data correction for CE-1 GRS.

#### 3.1 Channel Processing

Raw data transmitted from CE-1 are comprised of CCSDS (Consultative Committee for Space Data Systems) data frames, so the first step is channel processing (Fig. 3), which includes frame synchronization, descrambling, Reed-Solomon decoding, virtual channel data extraction and GRS data packet acquisition. It aims to acquire GRS raw packet data from CCSDS data frames.

##### (1) Frame Synchronization

Raw data that are received directly from CE-1 are comprised of CCSDS data frames. Frame synchronization is achieved with the aid of a sync pattern, which is either injected periodically into the data stream (continuous transmission) or appended at the beginning of each packet (packet transmission). Frame synchronization of the CE-1 raw data is achieved with the aid of a

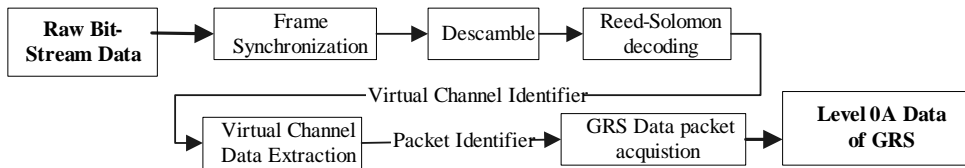


Fig. 3 Channel processing procedure.

sync pattern, which is appended at the beginning of each packet, and a sync pattern code is used to extract CCSDS data frames from raw bit-stream data.

(2) Descrambling

To assure the adequate change of channel density and avoid continuous 0 or 1 values for a long duration, data bits of each frame are scrambled at the transmitting end of a communication system with a pseudo-random sequence in the high-speed multi-channel multiplexer of the payload data management system (PDMS) onboard CE-1. At the receiving end of the Ground Research and Application System (GRAS), data bits of each frame are descrambled using the same pseudo-random bit pattern to recover the original data.

(3) Reed-Solomon Decoding

The moon is approximately 384 400 km from the earth, so channel errors are inevitably produced due to various kinds of interference factors. Thus, in the high-speed multi-channel multiplexer of the PDMS onboard CE-1, Reed-Solomon codes for correcting errors are used to reduce the channel errors. At the receiving end of the GRAS, a Reed-Solomon decoder extracted from the data stream is used to correct errors in the data frames.

(4) Virtual Channel Data Extraction

The Virtual Channel Data Units (VCDUs) are created to transmit eight sets of raw data acquired by CE-1. At the receiving end of the GRAS, virtual channel data are extracted on the basis of a virtual channel identifier in the CCSDS data frame.

(5) GRS data packet acquisition

After virtual channel data extraction, GRS data packets are extracted based on a GRS packet identifier in the CCSDS data frame from the virtual channel.

### 3.2 Optimal Data Selection

Optimal data selection (Fig. 4) includes the following steps:

- (1) The first step is where the processes of sequence sorting, splicing and removing duplicates are carried out on the GRS data packets from two data acquisition stations (the Miyun Station and the Kunming Station), respectively.

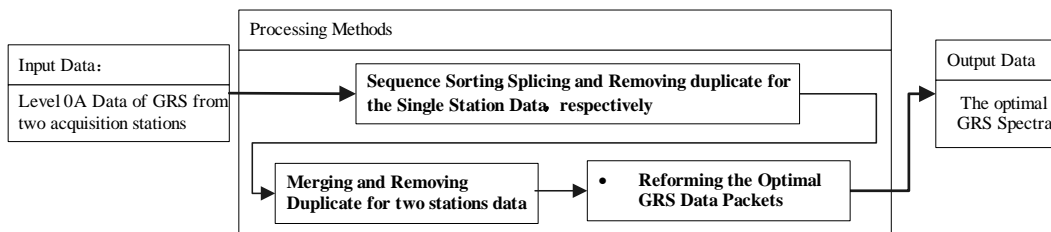


Fig. 4 Processing procedure for optimal data selection.

- (2) The second step is where merging, removing duplicates and forming the optimal data packets are carried out on the GRS data packets from two data acquisition stations.
- (3) The last step is that the optimal data packets are disassembled and reformed according to the structures of GRS data packets and scientific data blocks to acquire the optimal GRS spectra.

### 3.3 System Corrections

Using the results of the lab calibration and in-orbit calibration, a series of corrections are made to the optimal GRS spectra and are therefore referred to as system corrections. Below, we describe the three major system corrections: energy calibration, gain and dead time corrections.

#### 3.3.1 Energy Calibration

The goal of energy calibration is to convert channel spectra acquired by GRS to energy spectra. By measurements in the laboratory, we found that the relationship between channel and energy of the GRS detector is linear, so the linear relationship can be determined by fitting known characteristic energy values and their corresponding channel values acquired by measuring and analyzing gamma-rays emitted by the different characteristic energies. By using results from the experiment where the GRS measures gamma-ray spectra emitted by the calibrated gamma-ray sources (i.e.,  $^{57}\text{Co}$ ,  $^{137}\text{Cs}$ , and  $^{60}\text{Co}$ ) (Chang et al. 2009) and the radioactive sources in the laboratory (i.e.,  $^{40}\text{K}$  and  $^{208}\text{Tl}$ ), we can acquire gamma-ray spectra of the six characteristic energies that are 122, 662 keV, 1.17, 1.33, 1.46 and 2.615 MeV, respectively. The corresponding channel values of these six full energy peaks are obtained by the Gauss fitting of their characteristic energy spectra. The parameters  $a$  and  $b$  in the following equation are solved by fitting the above six pairs (channel versus energy) of data. Thus, the linear fitting result and the deviations between the measured and fitted energy are shown in Figure 5(left) and (right), respectively.

$$E1 = a \times \text{channel} + b, \quad (1)$$

where  $E1$  is the energy value, channel is the corresponding channel value of  $E1$ , and  $a$  and  $b$  are two fitting parameters that will be solved. By applying Equation (1), channel spectra observed by GRS are converted to energy spectra.

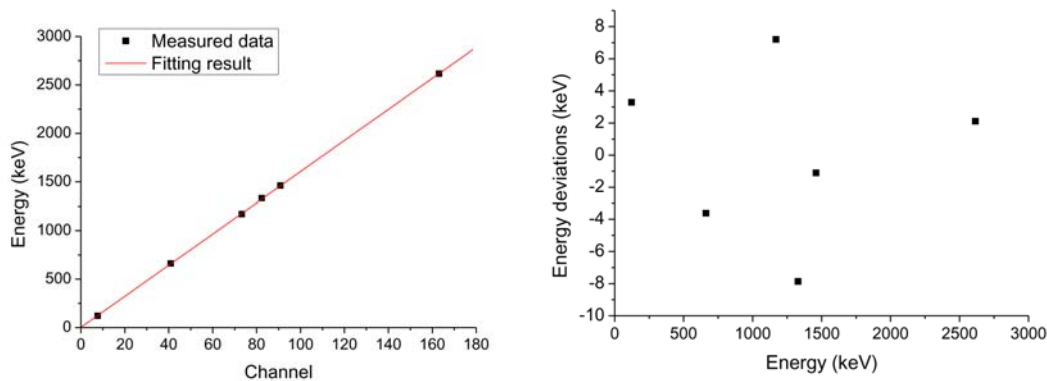


**Fig. 5** Left: plot of channel versus energy, right: energy deviations versus energy. By applying Equation (1), channel spectra observed by GRS are converted to energy spectra.

### 3.3.2 Gain Correction

Gain variations are caused by PMT changes and temperature changes. They can also result in channel shifts, so gain variations have to be monitored and corrected. The CE-1 GRS gain changes are monitored by analyzing the variation of the three characteristic peak positions including the 0.511 MeV annihilation peak, 6.13 MeV oxygen peak and 10.830 MeV nitrogen peak throughout the mission. Three peaks are clearly defined during the spacecraft's orbital period (127 minutes), and all the spectra detected in the lunar orbit are accumulated according to the spacecraft's orbital period. The three peak positions are obtained by performing Gauss fitting on the accumulated spectra for every spacecraft's orbital period. If the time variations of the peak positions are clear, we have to carry out gain corrections.

According to the above monitoring methods, we monitor the gain variations throughout the mission. We found that channel shift did not occur in the spectra detected by CE-1 GRS before 09:26:02 UTC on 2008 June 12. Since the static random access memory (SRAM) of the GRS failed at 02:30:27 UTC on 2008 July 3, gain corrections had to be carried out for spectra detected by CE-1 GRS during the period between 09:26:02 UTC on June 12 and 02:30:27 UTC on 2008 July 3.

The methods of gain corrections include 1) three peak positions are obtained for every 127-minute accumulated spectra throughout the mission; 2) the three peak positions for the first orbit of accumulated spectra are defined as the corresponding reference peak positions; 3) a linear relation is derived between the three reference peak positions and the corresponding peak positions for the other orbits of accumulated spectra; 4) the channels of spectra observed in other orbits are corrected by being recorded in the reference channels by using the linear relation built in the previous step; 5) the reference gain and offset values are obtained by linear fitting of the three pairs (reference channel vs. energy) for the first orbits of accumulated spectra; 6) the gain corrections for the other orbits of spectra are carried out by using the reference gain and offset values.

### 3.3.3 Dead Time Correction

Dead time of the prime detector can be caused by two reasons, which are cases where the prime detector is busy processing an event or the anticoincidence detector is busy processing an event. Based on the Lunar Prospector data analysis, we find that the count rate collected by the prime detector surrounding the moon is less than 1000 counts per second. By the GRS calibration tests in the laboratory, we find that the characteristic peak area at  $^{208}\text{Tl}$  (abbreviation of thallium) has little change when the count rate collected by the prime detector is less than 1000 gamma-ray counts per second. Hence, we can conclude that dead time caused by the prime detector being busy processing an event does not need to be corrected.

Dead time caused by the anticoincidence detector means that the spectra collected by the prime detector are affected by an anticoincidence square wave. In the ground calibration tests, the relative change of the peak area at  $^{208}\text{Tl}$  acquired by the prime detector is investigated when the different count rates are measured by the anticoincidence detector. Then the relation between the count rate of the anticoincidence detector and the relative change of the peak area at  $^{208}\text{Tl}$  is derived by the use of the experimental data. In the GRS data processing, the relative change is solved by using this relation derived from the ground tests and the count rate measured by the anticoincidence detector. Then, the counts observed by the prime detector divided by the relative change are the dead time corrected counts.

## 3.4 Geometric Corrections

The goals of geometric corrections are to obtain lunar positions of measured spectra and observation angles of the GRS detector by building the observation equation using the following information

such as the spacecraft ephemeris and attitude data, GRS installation parameters on the spacecraft, geometric parameters about the moon, etc. By using geometric corrections, we can obtain the geometric information including lunar surface longitude and latitude, orbit height, instrument incidence angle and azimuth angle at the moment of data acquisition.

The core of geometric positioning arithmetic is 1) to build the spatial triangle (Fig. 6) using three points including the CE-1 spacecraft's centroid, the moon's centroid and the lunar surface's observation point of GRS, which is formed by the GRS observation vector, the CE-1 position vector and the position vector of the lunar surface observation point, 2) to build the observation equation, and 3) to solve it.

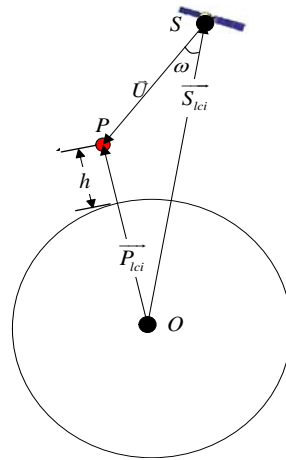


**Fig. 6** Spatial triangle formed by the observation vector ( $U$ ), the CE-1 position vectors ( $S$ ) and the position vectors of the lunar surface's observation point ( $P$ ).

The processing procedure for geometric corrections is shown in Figure 7. It mainly includes the three steps as follows:

(1) Data Preparation

Besides the system-corrected GRS spectra, data needed in geometric corrections include GRS installation parameters, spacecraft ephemeris and attitude data, geometric parameters about the moon, etc.

(2) The conversion of coordinate systems

Because the above input data needed for geometric corrections are defined under different coordinate systems, these input data must be converted into data under the identical coordinate system (CS). GRS installation parameters are defined under spacecraft body CS, spacecraft ephemeris and attitude data are defined under flat equatorial geocentric CS, and the lunar surface positions of the measured spectra obtained by geometric corrections are defined under lunar geodetic CS. To build the spatial triangle as shown in Figure 6, we must first carry out a series of coordinate conversions on the input data under different CSs so that the GRS observation vector and CE-1 position vector are converted into the vector under the lunar solid CS, respectively. The series of coordinate conversions are shown in Figure 7.

(3) Building the observation equation and deriving geometric information

After coordinate conversions, the observation equation is built based on the spatial triangle as shown in Figure 6 to solve the lunar positions and the relevant geometric parameters. In this paper, the process of establishing and solving the observation equation is abridged.

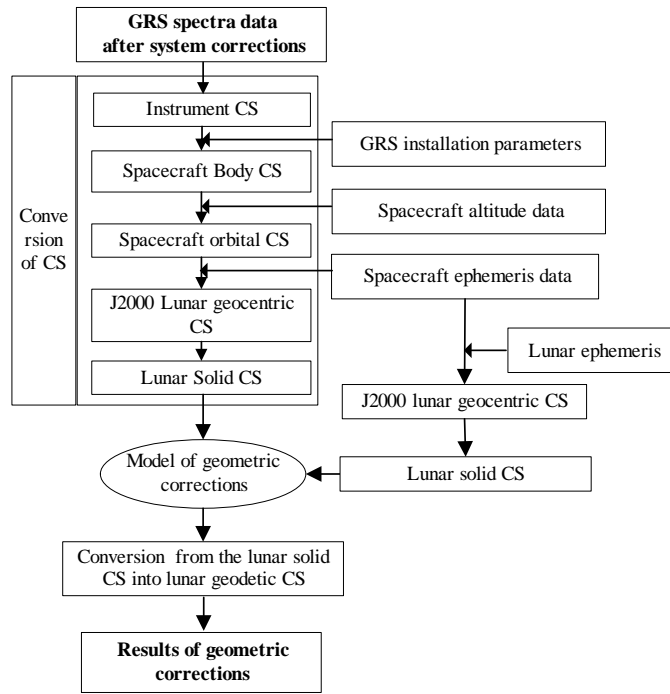


Fig. 7 Process of geometric corrections.

### 3.5 Orbit Altitude Normalization

Since the flux of the lunar gamma-rays is different at various spacecraft heights, we need to make corrections for variations of the lunar gamma-ray flux resulting from variations of the spacecraft height. In addition to the gamma-rays coming from the moon, there is a nonlunar component of gamma-rays coming from the galaxy (Lawrence et al. 2004). This nonlunar component does not vary with spacecraft height. It is measured using the background data that CE-1 GRS measured surrounding the moon. The variation of the lunar gamma-rays' flux acquired by the GRS at various spacecraft heights results from the variation of the Moon's solid angle as shown in Figure 8. The orbit altitude normalization performs the Moon's solid angle correction. Below, we describe how the moon's solid angle correction is carried out.

If we assume that the moon has a spherical surface, then the fractional solid angle relative to the surface varies with the spacecraft's altitude,  $h$ , and can be expressed using the following relation

$$\Omega(h) = \int_0^{2\pi} d\phi \int_0^{\theta_{\max}} \sin \theta d\theta = \int_0^{2\pi} d\phi \int_{\cos \theta_{\max}}^1 d(\cos \theta) = 2\pi(1 - \cos \theta_{\max}), \quad (2)$$

where  $\theta$  is the angle from the sub-spacecraft point to a visible location on the moon, and  $\theta_{\max} = \sin^{-1}(\frac{R_m}{R_m+h})$  is the maximum value that  $\theta$  can have for a given altitude. For simplification across data sets, we have normalized the solid angle of Equation (2) to the solid angle at the lunar surface, i.e.,  $\Omega'(h) = \Omega(h)/\Omega(0)$ . The full solid angle correction, including the non-lunar background, is then

$$\frac{C(h) - C_{\text{background}}}{C(0) - C_{\text{background}}} = \frac{\Omega(h)}{\Omega(0)} = \Omega'(h), \quad (3)$$

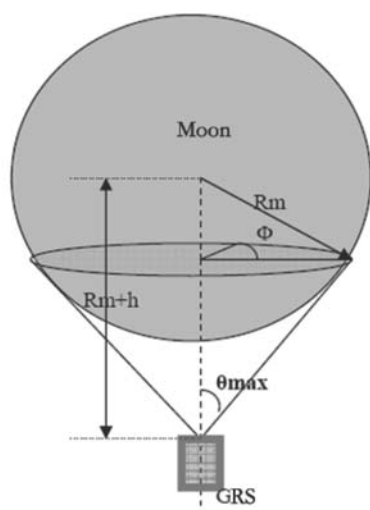


**Fig. 8** The moon's solid angle of GRS.

where  $C(h)$ ,  $C_{\text{background}}$  and  $C(0)$  are the uncorrected, background and solid angle corrected spectral counts, respectively.

Equation (3) now becomes

$$C(0) = \frac{C(h) - [1 - \Omega'(h)] C_{\text{background}}}{\Omega'(h)} = \frac{C(h) - \sqrt{1 - \left(\frac{R_m}{R_m+h}\right)^2} C_{\text{background}}}{1 - \sqrt{1 - \left(\frac{R_m}{R_m+h}\right)^2}}. \quad (4)$$

### 3.6 Eliminating Unusable Data

As for the orbit altitude normalized spectral data, the spectral data observed by GRS under the safe mode (that is 0 as the HV level) need to be eliminated to carry out the elemental abundance inversion. In the defining convention we adopt for the spectral quality status, if the first character is identified as "W" in quality status composed of the eight characters in one spectrum, this spectrum also needs to be eliminated. In addition, the following abnormal spectral data should be eliminated from the above nominal data sets: spectral measurements that show data are clearly off-limits (i.e., the spectrum measured at 06:49:09.060 UTC on 2008 December 28 in Fig. 9) and spectral measurements with geometric positioning errors (i.e., the geometric positioning results of the spectrum in Table 2).

**Table 2** One spectrum with abnormal geometric information

Field	Time	GRS Instrument status	Longitude	Latitude	Instrument incidence angle	Instrument azimuth angle	Spectrum with 512 channels	Quality status
Value	2007-12-07 T06:03:24.534Z	4 3 1	*	*	*	*	...	0X00EEFF

Notes: \* (=9999.9999) represents abnormal data.

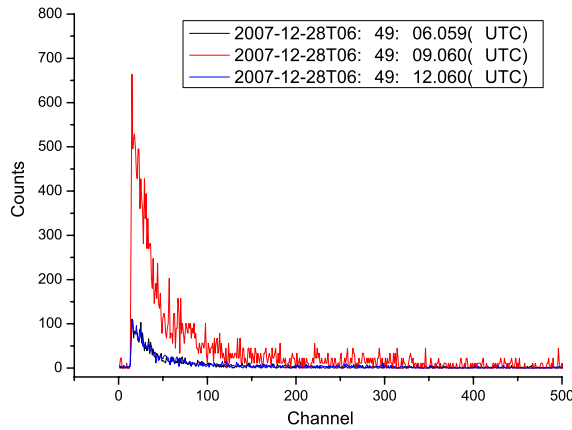


Fig. 9 One abnormal spectrum and two normal spectra.

### 3.7 Galactic Cosmic Ray Corrections

Since most of the primary and background gamma-rays being observed with the CE-1 GRS originate from galactic cosmic rays (GCRs) (the one exception is gamma-rays produced by radioactive decay), we need to monitor and correct for the time variability of the GCR flux. After much trial and error, we decided to monitor the time-varying GCR flux by measuring the counting rate in the 6.13 MeV oxygen gamma-ray line. This oxygen line is a good indicator of the GCR flux (Lawrence et al. 2004) because it is produced by inelastic scattering of fast neutrons, which are the direct product of the interaction of the GCR protons with the moon. In addition, since oxygen abundances should be mostly constant over the moon (Haskin & Warren 1991), the time variation of the 6.13 MeV oxygen line should be dominated by GCR flux variations.

Since there are oxidants in the remaining propulsion fuel in the spacecraft after maneuvering into orbit around the moon, the 6.13 MeV oxygen gamma-rays come from the remaining propulsion fuel in addition to the lunar surface. During the period of the GRS data acquisition, less than 20 kg of fuel was consumed and the vast majority of consumed fuel was used in spacecraft maneuvers. Below, we carry out the comparative analysis on variation of the 6.13 MeV oxygen line before and after spacecraft maneuvers. The variation of the 6.13 MeV oxygen line before and after the orbit maintenance is shown in Figure 10. The variation of the 6.13 MeV oxygen line is shown in Figure 11 before and after the spacecraft's attitude trim. From Figures 10 and 11, we can find that there are little variations of the 6.13 MeV oxygen line in two spacecraft maneuvers. Therefore, we decided to monitor the time-varying GCR flux by measuring the counting rate in the 6.13 MeV oxygen line.

In order to apply the GCR corrections, we have smoothed the 6.13 MeV line's counting rate over 127 minutes (one orbit of GRS spectral data) and normalized them to the counting rate seen at the beginning of the orbital mission on 2007 December 29. The processes of the GCR corrections include, 1) the 6.13 MeV line's counting rate during the first orbit of the valid spectra of the GRS orbital mission is smoothed and selected as the reference data; 2) the 6.13 MeV line's counting rates during the other orbits of the valid spectra of the GRS orbital mission are smoothed and defined as the uncorrected data; 3) the relation between uncorrected data and the reference data is defined as a linear relation; 4) the uncorrected data are corrected using the above linear function built in step 3).

Figure 12 shows the uncorrected and corrected counts of the 556th~705th orbit of GRS data. From Figure 12, the corrected data show better correction results.

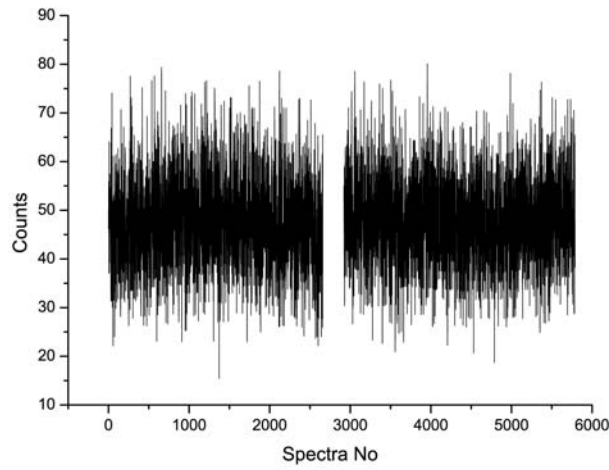


**Fig. 10** Variation of the 6.13 MeV oxygen line before and after the orbit maintenance.

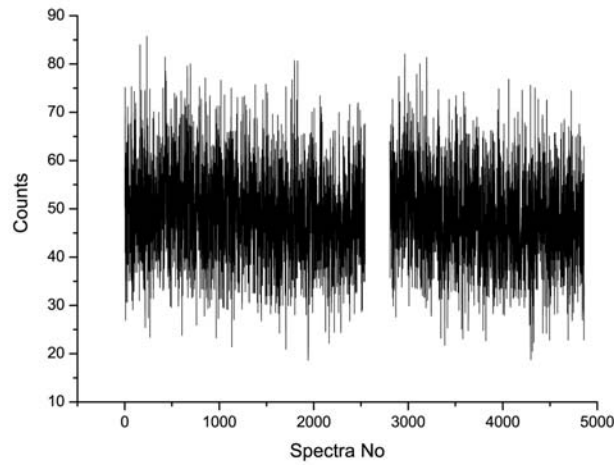


**Fig. 11** Variation of the 6.13 MeV oxygen line before and after spacecraft attitude trim.

#### 4 DATA UNCERTAINTIES

Besides the uncertainties due to Poisson statistics, non-Poisson uncertainties are responsible for the measured spectral uncertainties. All of the time series corrections described in this paper are carried out in order to reduce non-Poisson uncertainties in the CE-1 GRS data. The ultimate goal is to reduce the uncertainties to the level of Poisson uncertainties. One way to quantify uncertainties (Lawrence et al. 2004) is to map the data onto equal-area pixels and measure the standard deviation for each pixel using the following equation

$$\sigma_{\text{measured}} = \sqrt{\frac{\sum_{i=0}^{N_{\text{spectra}}} (S_i - S)^2}{N_{\text{spectra}} - 1}}, \quad (5)$$

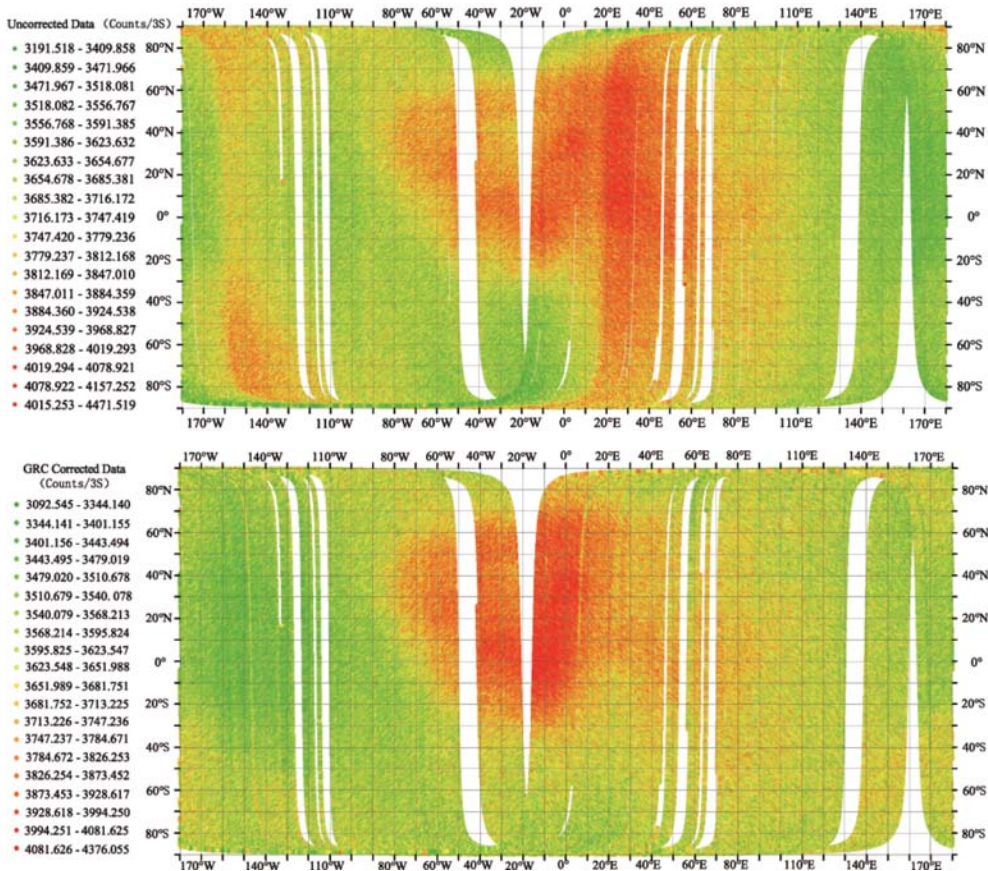


**Fig. 12** *Top panel:* the uncorrected count distribution; *bottom panel:* the GCR corrected count distribution.

where  $N_{\text{spectra}}$  is the number of accumulated spectra in each pixel,  $S$  is the mean counts measured per three seconds in each pixel, and  $S_i$  is the measured counts in a given 3s spectrum  $i$ . The fractional standard deviation is then  $\sigma_{\text{measured}}/S$ .

By examining a plot of measured uncertainty of uncorrected data versus the Poisson uncertainty, we can see what impact the non-Poisson uncertainties have on the raw data observed by CE-1 GRS. From a plot of measured uncertainty of the time series corrected data versus the Poisson uncertainty, we can also see to what extent the non-Poisson uncertainties in raw data observed by CE-1 GRS are reduced by the time series data correction (Lawrence et al. 2004).

## 5 CONCLUSIONS

In this paper, detailed discussions are given on the time series data correction procedures and methods for the CE-1 GRS.

- (1) We discuss how to acquire GRS raw packets from raw bit-stream data transmitted from CE-1 by channel processing. In channel processing, the methods of frame synchronization, descrambling, Reed-Solomon decoding and GRS raw packet acquisition are described.

- (2) The methods of the optimal GRS raw packet selection are discussed because GRS raw packets transmitted from CE-1 are simultaneously acquired by two data acquisition stations (Miyun station and Kunming Station).
- (3) The methods of energy calibration, gain and dead time corrections are presented based on the results of the lab calibration and in-orbit calibration.
- (4) We discuss how to acquire lunar positions of the measured spectra and observation angles of the GRD. They are acquired by building the observation equation using information such as spacecraft ephemeris and attitude data, GRS installation parameters on the spacecraft, geometric parameters about the moon, etc.
- (5) The method for correcting variations in the lunar gamma-ray flux resulting from variations of the spacecraft's orbit altitude is described.
- (6) We discuss the method for correcting the time variability of the GCR flux. After much trial and error, we selected the 6.13 MeV oxygen line to monitor the time-varying GCR flux, and better results of GCR corrections were obtained.

**Acknowledgements** The authors would like to thank all the CE-1 GRS team members for their outstanding work. The authors are very thankful for the constructive comments and suggestions from the two anonymous reviewers. This work is supported by the National High Technology Research and Development Program of China (Grant Nos. 2008AA12A212 and 2010AA122202) and the National Natural Science Foundation of China (Grant Nos. 41040031 and 40904024).

## References

- Chang, J., Ma, T., Zhang, N., et al. 2009, in Proc. Int. Workshop Advances in Cosmic Ray Science, J. Phys. Soc. Jpn., 78 (Suppl. A), 26
- Haskin, L. A., & Warren, P. 1991, Lunar chemistry, in Lunar Sourcebook, eds. Heiken, G. H., et al., (New York: Cambridge Univ. Press), 357
- Lawrence, D. J., Feldman, W. C., Barraclough, B. L., et al. 1998, Science, 281, 1484
- Lawrence, D. J., Maurice, S., & Feldman, W. C. 2004, Journal of Geophysical Research (Planets), 109, 7
- Metzger, A. E. 1993, Composition of the Moon as determined from orbit by gamma-ray spectroscopy (New York: Cambridge Univ. Press), 341
- Metzger, A. E., Haines, E. L., Etchegaray-Ramirez, M. I., & Hawke, B. R. 1979, in Lunar and Planetary Science Conference Proceedings, ed., N. W. Hinners, 10, 1701
- Metzger, A. E., Haines, E. L., Parker, R. E., & Radocinski, R. G. 1977, in Lunar and Planetary Science Conference Proceedings, ed. R. B. Merrill, 8, 949
- Metzger, A. E., Trombka, J. I., Reedy, R. C., & Arnold, J. R. 1974, in Lunar and Planetary Science Conference Proceedings, 5, 1067
- Prettyman, T. H., Hagerty, J. J., Elphic, R. C., et al. 2006, Journal of Geophysical Research (Planets), 111, 12007